

Zero Temperature Thermodynamics of Asymmetric Fermi Gases at Unitarity

Aurel Bulgac and Michael McNeil Forbes

Department of Physics, University of Washington, Seattle, WA 98195-1560

(Dated: 27 March 2007)

The equation of state of a dilute two-component asymmetric Fermi gas at unitarity is subject to strong constraints, which affect the spatial density profiles in atomic traps. These constraints require the existence of at least one non-trivial partially polarized (asymmetric) phase. We determine the relation between the structure of the spatial density profiles and the $T = 0$ equation of state, based on the most accurate theoretical predictions available. We also show how the equation of state can be determined from experimental observations.

PACS numbers: 03.75.Ss

We consider the $T = 0$ thermodynamics of a dilute asymmetric Fermi gas comprising two species of equal mass with s -wave interactions at unitarity. This has been recently realized in ${}^6\text{Li}$ experiments [1–4]. We shall discuss the phase structure in the microcanonical and grand-canonical ensembles, and its manifestation in cold atomic traps using the local density approximation (LDA). The theoretical treatment of the grand-canonical ensemble is much simpler than the microcanonical ensemble as it consists of only pure phases. We discuss here the most general model-independent equation of state satisfying known constraints. For model-dependent analyses see [5–7].

a. Phase structure: We show the main defining features of a grand-canonical phase diagram in Fig. 1. The two species are labelled “ a ” and “ b ”. The symmetry $a \leftrightarrow b$ allows us to consider only the region below the $\mu_a = \mu_b$ line where the locally averaged number densities and chemical potentials satisfy $n_b \leq n_a$ and $\mu_b \leq \mu_a$ respectively. The asymmetry of the system may thus be characterized by the dimensionless ratios:

$$x = n_b/n_a \leq 1, \quad y = \mu_b/\mu_a \leq 1. \quad (1)$$

Note that only x measures a physical asymmetry. There are four distinct regions: Vac—the vacuum, N_a —the fully polarized phases ($x = 0$) comprising only species “ a ”, PP_a —partially polarized phase(s) ($0 < x < 1$), and SF—the fully paired symmetric superfluid phase ($x = 1$).

We shall discuss only two phase transitions: one between the fully polarized phase N_a (where $x = 0$) and a partially polarized phase PP_a ($0 < n_b < n_a$), and another between a (possibly different) partially polarized phase and the symmetric fully paired phase SF (where $x = 1$). At unitarity, phase transitions occur along rays characterized solely by their slope y_x . The two transitions we shall discuss are thus described by the two universal parameters y_0 and y_1 , which naturally satisfy $y_0 \leq y_1$. A major point of this paper is to place an upper bound Y_0 on y_0 ($y_0 \leq Y_0$), a lower bound Y_1 on y_1 ($Y_1 \leq y_1$), and to show $Y_0 < Y_1$, which implies that the inequality $y_0 < y_1$ is strict. This directly implies the existence and stability of one or more partially polarized phase(s) PP_a . Possible phases in the region PP_a include LOFF states [10], states with deformed Fermi surfaces [11], and p -wave superfluid

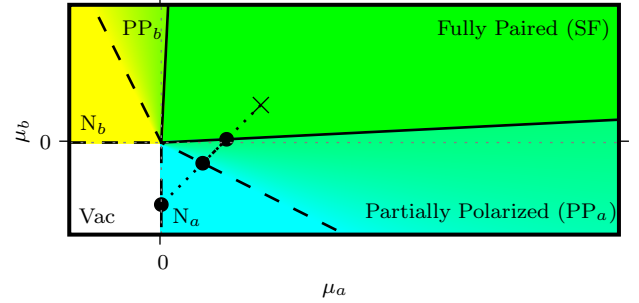


FIG. 1: Grand-canonical phase diagram of a two-component Fermi gas at unitarity and $T = 0$. Various phases are separated by phase transitions along the straight lines extending from the origin with constant slopes y_x . The dotted line follows the sequence of phases in a sample trap.

states [12]. If several of these states exists and are stable, the corresponding phase transitions will be characterized by additional universal parameters y_x .

b. Functional forms of thermodynamic potentials: At unitarity, the energy density $\mathcal{E}(n_a, n_b)$ and the pressure $\mathcal{P}(\mu_a, \mu_b)$ have the following form:

$$\mathcal{E}(n_a, n_b) = \frac{3}{5}\alpha [n_a g(x)]^{5/3}, \quad \alpha = \frac{(6\pi^2)^{2/3} \hbar^2}{2m}, \quad (2a)$$

$$\mathcal{P}(\mu_a, \mu_b) = \frac{2}{5}\beta [\mu_a h(y)]^{5/2}, \quad \beta = \frac{1}{6\pi^2} \left[\frac{2m}{\hbar^2} \right]^{3/2}. \quad (2b)$$

Note that $g(x) = f^{3/5}(x)$, where $f(x)$ was introduced in [8]: The use of $g(x)$ rather than $f(x)$ significantly simplifies the formalism [9]. The $T = 0$ thermodynamic properties of the system are completely determined by the functional form of $g(x)$ or $h(y)$. The number densities and chemical potentials are simply $n_{a,b} = \partial\mathcal{P}/\partial\mu_{a,b}$ and $\mu_{a,b} = \partial\mathcal{E}/\partial n_{a,b}$ respectively. As we show here, the functions $h(y)$ and $g(x)$ are tightly constrained by current Monte Carlo simulations, analytic calculations, and experimental results. The energy density and pressure are related via the Legendre transform [9]:

$$\mathcal{P}(\mu_a, \mu_b) = \mu_a n_a + \mu_b n_b - \mathcal{E}(n_a, n_b) = \frac{2}{3}\mathcal{E}(n_a, n_b). \quad (3)$$

c. Physical constraints: The thermodynamics of three phases are known. The vacuum has vanishing pressure $\mathcal{P}_{\text{Vac}} = 0$, the fully polarized phase N_a is a free Fermi gas,

$$\mathcal{P}_{\text{FG}}(\mu_a) = \frac{2}{5}\beta\mu_a^{5/2}, \quad (4)$$

and the pressure of the fully paired phase SF is symmetric in μ_a and μ_b , and is described by a single parameter ξ ,

$$\mathcal{P}_{\text{SF}}(\mu_{\pm}) = \frac{4}{5} \frac{\beta}{\xi^{3/2}} \mu_{\pm}^{5/2} \quad \text{where} \quad \mu_{\pm} = \frac{\mu_a \pm \mu_b}{2}. \quad (5)$$

These provide the limiting forms for $h(y)$ and limiting values of $g(x)$, [see Eqs. (6a) and (7a) below].

The phase transition at $y = y_0$ defines the border of the region where $\mu_b = y_0\mu_a$ is tuned to keep species “ b ” out of the system. Since the interspecies interaction is attractive, the critical μ_b must be negative $y_0 < 0$. We will provide an upper bound Y_0 ($y_0 \leq Y_0$).

Note that $\mathcal{P}_{\text{SF}}(\mu_{\pm})$ depends only on the average chemical potential μ_{\pm} . This insensitivity to the chemical potential difference μ_{-} is due to the existence of an energy gap Δ in the spectrum. The phase transition at $y = y_1$ marks the line where μ_{-} becomes large enough to break the superfluid pairs. In the phase SF, μ_{-} is constrained by the size of the physical gap $\mu_{-} \leq \Delta$ [8]. This provides a lower bound $Y_1 \leq y_1$, see below and [9].

(Recall from Eq. (1) that we are only considering regions where $0 \leq \mu_{-} = |\mu_{-}|$).

If no stable partially polarized phase exists, then the region PP_a will vanish, being compressed into a single first-order transition line where pressure equilibrium is established $\mathcal{P}_{\text{FG}}(\mu_a) = \mathcal{P}_{\text{SF}}(\mu_{\pm})$ [6, 8]. This would occur at $y = y_c = (2\xi)^{3/5} - 1 \equiv y_0 \equiv y_1$, and would imply that $Y_0 \equiv Y_1$. We argue below that Y_0 is strictly less than Y_1 , and therefore rule out this possibility.

Finally, thermodynamic stability requires that the pressure and energy density are convex functions, which implies that $g(x)$ and $h(y)$ are also convex [9]. The constraints on $h(y)$ are

$$h(y) = \begin{cases} 1 & \text{if } y \leq y_0, \\ (1+y)(2\xi)^{-3/5} & \text{if } y \in [y_1, 1], \end{cases} \quad (6a)$$

$$h''(y) \geq 0, \quad \text{and} \quad (6b)$$

$$y_0 \leq Y_0 < y_c < Y_1 \leq y_1 \leq 1. \quad (6c)$$

The corresponding constraints on $g(x)$ are

$$g(0) = 1, \quad g(1) = (2\xi)^{3/5}, \quad (7a)$$

$$g''(x) \geq 0, \quad \text{and} \quad (7b)$$

$$g'(0) \leq Y_0, \quad g'(1) \in [g(1)(1+Y_1^{-1})^{-1}, g(1)/2]. \quad (7c)$$

Equation (6a) follows directly from Eqs. (2b), (4), and (5), Eq. (7a) follows from Eq. (2a), and the interval in Eq. (7c) follows from the properties of the Legendre transform and Eq. (6c) [9].

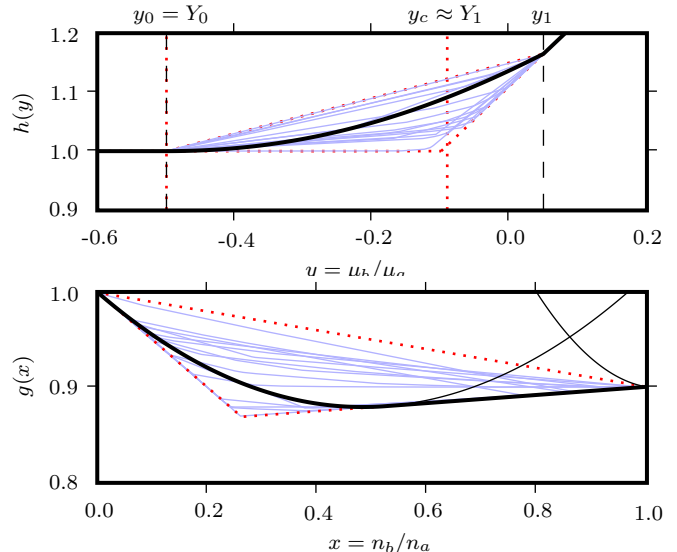


FIG. 2: Example of a function $h(y)$ and the corresponding function $g(x)$ shown as thick lines. Maxwell’s construction for phase coexistence leads to a linear $g(x)$ for $x \in (0.5, 1.0)$, interpolating between the two pure phases shown with lighter lines. This corresponds to the kink (first-order phase transition) at $y = y_1$ in $h(y)$. Various other sample functions are lightly sketched within the allowed (dotted) triangular region.

d. Parameters: For Fig. 2 we used

$$\xi = 0.42(1), \quad Y_0 \approx -0.5, \quad Y_1 = -0.09(3), \quad y_1 = 0.05.$$

We obtain estimates for Y_1 and ξ from Monte Carlo data [13–15]. The latest Monte Carlo estimates for the symmetric systems give $\xi = 0.42(1)$ [14, 15] and $\Delta/\varepsilon_{\text{F}} = 0.504(24)$ [15], where ε_{F} is the Fermi energy of the free gas with the same density. This gives $y_c \approx -0.099(15)$, and the constraint $\mu_{-} \leq \Delta$ gives $Y_1 = (\xi - \Delta/\varepsilon_{\text{F}})/(\xi + \Delta/\varepsilon_{\text{F}}) = -0.09(3)$ [8, 9]. Since within the statistical errors $Y_1 \approx y_c$, the possibility of an empty PP_a region at unitarity cannot yet be ruled out by this value of Y_1 , as was noted earlier by Cohen [8].

We now estimate Y_0 . Let e_0 be the energy required to add one particle b to a fully polarized gas of density n_a . Consider adding a large, but infinitesimal amount of b , $1 \ll N_b \ll N_a$. In the thermodynamic limit, the required energy per particle will be the critical chemical potential $\mu_b = \alpha n_a^{2/3} g'(0)$ defining the transition y_0 . If the added particles repel, the energy will be $N_b e_0$, and $\mu_b = e_0$. If they bind, the additional binding energy must be included, giving $\mu_b < e_0$. In this way, e_0 provides a bound for μ_b and $g'(0) = y_0 \leq Y_0 = e_0/(\alpha n_a^{2/3})$.

Consider adding a single b fermion, with coordinate \mathbf{r}_0 , to a system of N_a a fermions with coordinates \mathbf{r}_n . Let $r_{nm} = |\mathbf{r}_n - \mathbf{r}_m|$. The wave function for the b fermion in the background of fixed a sources is

$$\phi(\mathbf{r}_0; \{\mathbf{r}_n\}) = \sum_n A_n \frac{\exp(-\kappa r_{0n})}{r_{0n}}, \quad (8)$$

and it satisfies the zero-range interaction boundary conditions if the following N_a conditions are met:

$$\left(-\kappa + \frac{1}{a}\right) A_n + \sum_{m \neq n} A_m \frac{\exp(-\kappa r_{nm})}{r_{nm}} = 0. \quad (9)$$

For uniform distributions where the lowest state has constant $A_m = A$, approximating the sum as an integral gives $\kappa - a^{-1} = 4\pi n_a / \kappa^2$. This continuum approximation is not very accurate in the unitary limit, since κ is comparable to the inverse interparticle spacing and $\kappa^3 / n_a \approx 4\pi$. To estimate corrections, the equations can be solved for various lattice configurations. We find that κ deviates from the continuum result by a factor of 0.84(3) for simple lattice configurations and perturbations (see [9] for details). We now estimate the energy of the system using the wave function

$$\Psi(\mathbf{r}_0; \{\mathbf{r}_n\}) = \Phi_{\text{SD}}(\{\mathbf{r}_n\}) \phi(\mathbf{r}_0; \{\mathbf{r}_n\}), \quad (10)$$

where Φ_{SD} is a Slater determinant for a free Fermi gas and obtain $e_0 \approx -\hbar^2 \kappa^2 / m$ [9]:

$$e_0 \approx \begin{cases} 4\pi \hbar^2 n_a a / m, & \text{if } a \rightarrow 0^-, \\ -0.71(5) \hbar^2 (4\pi n_a)^{2/3} / m, & \text{if } a \rightarrow \pm\infty, \\ -\hbar^2 / (ma^2), & \text{if } a \rightarrow 0^+. \end{cases} \quad (11)$$

Note that this result interpolates between the correct leading order BEC and BCS results. This estimate assumes that the fluctuations of the number density $n_a(\mathbf{r})$ on a scale of the order $1/\kappa$ affect κ very little. The result is consistent with this assumption, as discussed in [9]. The constraint at unitarity is thus

$$Y_0 \approx -0.54(4) < y_c = -0.099(15). \quad (12)$$

If Y_0 is strictly less than y_c , then convexity in $g(x)$ and $h(y)$ implies $y_c < Y_1$ (see Fig. 2).

e. Trap profiles: For large systems with a slowly varying confining potential, gradient terms may be neglected, and the LDA employed to determine the density distribution by introducing spatially varying effective chemical potentials:

$$\mu_{a,b}(\mathbf{R}) = \lambda_{a,b} - V(\mathbf{R}). \quad (13)$$

Lagrange multipliers $\lambda_{a,b}$ fix the total particle numbers N_a and N_b . The LDA may be inaccurate near phase boundaries where the densities change rapidly. The gradient terms will smear out these transition regions and provide an additional surface tension proportional to the local curvature [16].

In the LDA, the density profile may be constructed from the local densities $n_{a,b}$ using Eq. (13) (explicit formulae are provided in [9]). The dotted line in Fig. 1 shows the sequence of phases contained in a sample trap. Since $2\mu_- = \lambda_a - \lambda_b$ is fixed, traps contain the sequence of phases encountered along a 45° line through such a diagram. In this example, the center of the cloud

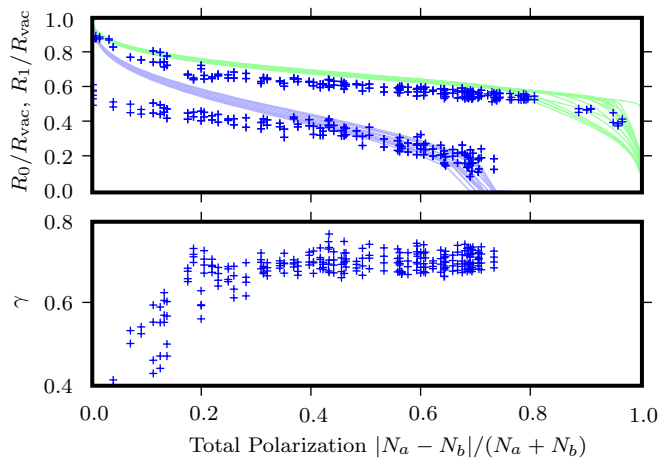


FIG. 3: Measured transition radii from Ref. [3]. The upper plot shows the normalized data (crosses) on top of data generated from several randomly generated functions $h(y)$. The lower plot shows the parameter γ defined in Rel. (14).

($V(\mathbf{0}) = 0$) is in the SF phase at the cross. The phase transitions will occur for $y = y_1$, $y = y_0$, and $y = -\infty$ for $V(\mathbf{R}_1) = V_1$, $V(\mathbf{R}_0) = V_0$, and $V(\mathbf{R}_{\text{vac}}) = V_{\text{vac}}$ respectively, with $R_0 < R_1 < R_{\text{vac}}$. As noted above, additional phase transitions may exist between R_0 and R_1 .

f. Experiments: Accurate measurements of the density profiles would allow for a complete extraction of $h(y)$ and $g(x)$. For example, using $x = n_b(\mathbf{R})/n_a(\mathbf{R})$ and the expressions for $\mu_{a,b}$, we have $g^{2/3}(x)g'(x) = [\lambda_b - V(\mathbf{R})]/[\alpha n_a^{2/3}(\mathbf{R})]$ from which $g(x)$ may be extracted using the boundary condition $g(0) = 1$ [9].

For harmonic traps, the locations of the main phase transitions, $R_{\text{vac}} \propto \sqrt{V_{\text{vac}}}$, $R_0 \propto \sqrt{V_0}$, and $R_1 \propto \sqrt{V_1}$, are completely determined by the Lagrange multipliers $\lambda_{a,b}$, and the universal numbers y_0 and y_1 . Within the LDA, we obtain the following model independent relationship, to be compared with the recent MIT data [3] (see Fig. 3):

$$\gamma = \frac{1 - y_1}{1 - y_0} = \frac{R_{\text{vac}}^2 - R_0^2}{R_{\text{vac}}^2 - R_1^2} \approx 0.70(5). \quad (14)$$

To extract more information, one must consider a specific functional form for $h(y)$ and $g(x)$. We have analyzed a large sample of allowed functions $h(y)$ and $g(x)$, a few of which are sketched in Figs. 2 and 3. We find that the total polarization $P = (N_a - N_b)/(N_a + N_b)$ is quite insensitive to the functional form. However, the critical polarization P_c —where the innermost phase transition approaches the center of the trap $R_1 = 0$ —is quite sensitive to y_1 . The MIT experiments [1, 3] measure $P_c = 0.70(5)$. If $y_1 = 0$, then one obtains $P_c > 0.80 \dots 0.85$. However, if one considers $y_1 \approx 0.05$ ($g'(1) \approx 0.04$), then values of $P_c \approx 0.7$ and smaller emerge, compatible with those measured in [1, 3]. Using Eq. (14), this gives a value of $y_0 = g'(0) \approx -0.4$. Our estimate for $Y_0 \approx -0.54(4)$ is consistent with this extracted experimental value within existing uncertainties.

Within the Eagles-Leggett extension of the BCS model [17], one obtains the values $y_0 = 0$, $y_c = 0.105$, and $y_1 = 0.107$ (see [7, 9]), which would correspond to a parameter $\gamma = 0.893$, as opposed to the $\gamma = 0.70(5)$ extracted from experiment. At the same time, the spatial layer for the PP_a region would be very thin, namely $(R_0^2 - R_1^2)/(R_{\text{vac}}^2 - R_1^2) = 1 - \gamma = 0.107$, compared with our estimate $1 - \gamma \approx 0.30(5)$.

Our analysis is strictly valid only at $T = 0$. The deviations in Fig. 3 are most likely finite temperature effects. The regions of the phase diagram most sensitive to $T \neq 0$ are those with small μ , thus, the transition radii in traps with small asymmetry will be most affected. For large polarizations, the temperature should not affect the SF phase which is gapped, but will affect phases with zero or small gap excitations. This could alter the values of y_1 slightly and y_0 significantly. We thus caution against taking the extracted numbers in this section too seriously until a similar finite temperature analysis is presented.

Since $Y_1 < 0$ (as determined from the value of the pairing gap), a positive y_1 suggests a first-order phase transition out of the SF phase for a critical $\mu_- < \Delta$. This conclusion is also consistent with the form of the quasi-particle spectrum computed in [15], which has a minimum at a finite momentum.

In conclusion, we have shown that thermodynamic con-

straints, accurate Monte Carlo simulations, analytic estimates, and experimental data place tight constraints on the equation of state of the asymmetric $T = 0$ unitary gas. These constraints imply that there exists a region where *one or more nontrivial partially polarized phases exist*. These phases likely exhibit very interesting microscopic physics. In particular, any ungapped polarized phase is unstable towards the formation of a state with two symbiotic superfluids at $T = 0$ [12]. The tight constraints on the forms of $g(x)$ and $h(y)$ we present will help locate these novel phases.

The authors thank A. Schwenk and M. W. Zwierlein for comments, D. T. Son for many useful discussions, M. W. Zwierlein *et al.* for providing the data in Fig. 3, and the US Department of Energy for support under Grant No. DE-FG02-97ER41014.

Notes added: Chevy [18] independently arrived at similar conclusions. The latest MIT analysis [19] agrees with our conclusion that the SF phase occupies the center of the trap and shows that the LDA is applicable. In a recent variational Monte Carlo study, Lobo *et al.* [20] agree with our lower bound, obtaining $Y_0 = -0.58(1) < y_c = -0.099(15)$, and concluded that the transition at y_1 is first-order. This is consistent with our results: their function $f(x)$ is very similar to our $g^{5/3}(x)$ (see [9]).

-
- [1] M.W. Zwierlein, A. Schirotzek, C.H. Schunck, and W. Ketterle, *Science* **311**, 492 (2006), arXiv:cond-mat/0511197.
- [2] G.B. Partridge, W. Li, R. I. Kamar, Y. an Liao, and R. G. Hulet, *Science* **311**, 503 (2006), arXiv:cond-mat/0511752.
- [3] M.W. Zwierlein, C.H. Schunck, A. Schirotzek, and W. Ketterle, *Nature (London)*, **442**, 54 (2006), arXiv:cond-mat/0605258.
- [4] M.W. Zwierlein and W. Ketterle, *Science*, 314, 54 92006 (2006), arXiv:cond-mat/0603489; G.B. Partridge, W. Li, R. I. Kamar, Y. an Liao, and R. G. Hulet, *Science*, 314, 54 (2006), arXiv:cond-mat/0605581.
- [5] P.F. Bedaque, H. Caldas, and G. Rupak, *Phys. Rev. Lett.* **91**, 247002 (2003), arXiv:cond-mat/0306694; T. Mizushima, K. Machida, and M. Ichioka, *ibid.* **94**, 060404 (2005), arXiv:cond-mat/0409417; J. Kinnunen, L.M. Jensen, and P. Törmä, *ibid.* **96**, 110403 (2006), arXiv:cond-mat/0512556; W. Yi and L.-M. Duan, *Phys. Rev. A* **73**, 031604(R) (2006), arXiv:cond-mat/0601006; M. Iskin and C.A.R. Sa de Melo, *Phys. Rev. Lett.* **97**, 100404 (2006), arXiv:cond-mat/0604184; K. Machida, T. Mizushima, and M. Ichioka, *ibid.* **97**, 120407 (2006), arXiv:cond-mat/0604339; L.M. Jensen, J. Kinnunen, and P. Törmä, arXiv:cond-mat/0604424; C.-C. Chien, Q. Chen, Y. He, and K. Levin, *Phys. Rev. Lett.* **97**, 090402 (2006), arXiv:cond-mat/0605039; W.-C. Su, arXiv:cond-mat/0511183; L. He, M. Jin, and P. Zhuang, *Phys. Rev. B* **73**, 214527 (2006), arXiv:cond-mat/0601147; X.-J. Liu and H. Hu, *Europhys. Lett.* **75** 364 (2006), arXiv:cond-mat/0603011; C.-H. Pao and S.-K. Yip, *J. Phys.: Condens. Matter* **18** 5567 (2006), arXiv:cond-mat/0604530; M. M. Parish, F. M. Marchetti, A. Lamacraft, and B. D. Simons, *Nature Physics* **3**, 124 (2007), arXiv:cond-mat/0605744.
- [6] F. Chevy, *Phys. Rev. Lett.* **96**, 130401 (2006), arXiv:cond-mat/0601122.
- [7] M. Haque and H.T.C. Stoof, *Phys. Rev. A* **74**, 011602 (2006), arXiv:cond-mat/0601321.
- [8] T.D. Cohen, *Phys. Rev. Lett.* **95**, 120403 (2005), arXiv:cond-mat/0501080.
- [9] See the appendix or EPAPS Document No. for additional calculational details. For more information on EPAPS, see <http://www.aip.org/pubservs/epaps.html>.
- [10] P. Fulde and R. A. Ferrell, *Phys. Rev.* **135**, A550 (1964). A.I. Larkin and Y.N. Ovchinnikov, *Sov. Phys. JETP* **20**, 762 (1965).
- [11] H. Müther and A. Sedrakian, *Phys. Rev. Lett.* **88**, 252503 (2002), arXiv:cond-mat/0202409.
- [12] A. Bulgac, M.M. Forbes, and A. Schwenk, *Phys. Rev. Lett.* **97**, 020402 (2006), arXiv:cond-mat/0602274.
- [13] J. Carlson, S.Y. Chang, V.R. Pandharipande, and K.E. Schmidt, *Phys. Rev. Lett.* **91**, 050401 (2003), arXiv:physics/0303094; S.Y. Chang, V.R. Pandharipande, J. Carlson, and K.E. Schmidt, *Phys. Rev. A* **70**, 043602 (2004), arXiv:physics/0404115.
- [14] G.E. Astrakharchik, J. Boronat, J. Casulleras, and S. Giorgini, *Phys. Rev. Lett.* **93**, 200404 (2004), arXiv:cond-mat/0406113.
- [15] J. Carlson and S. Reddy, *Phys. Rev. Lett.* **95**, 060401 (2005), arXiv:cond-mat/0503256.

- [16] T.N. De Silva and E.J. Mueller, Phys. Rev. Lett. **97**, 070402 (2006), arXiv:cond-mat/0604638; A. Imambekov, C.J. Bolech, M. Lukin, and E. Demler, Phys. Rev. A **74**, 053626 (2006), arXiv:cond-mat/0604423.
- [17] D.R. Eagles, Phys. Rev. **186**, 456 (1969); A.J. Leggett, in *Modern Trends in the Theory of Condensed Matter*, edited by A. Pekalski and R. Przystawa, (Springer-Verlag, Berlin, 1980); J. Phys. (Paris) Colloq. **41**, C7 (1980).
- [18] F. Chevy, arXiv:cond-mat/0605751.
- [19] Y. Shin, M.W. Zwierlein, C.H. Schunck, A. Schirotzek, and W. Ketterle, Phys. Rev. Lett. **97**, 030401 (2006), arXiv:cond-mat/0606432.
- [20] C. Lobo, A. Recati, S. Giorgini and S. Stringari, Phys. Rev. Lett. **97**, 200403 (2006), arXiv:cond-mat/0607730.

APPENDIX A: ADDITIONAL DETAILS

In this appendix, we present some additional calculational details. We discuss the properties of the Legendre transformation, thermodynamic stability and convexity of thermodynamic potentials, and the Maxwell construction for mixed phases. We also provide details of the calculations whose results are presented in the main body.

1. Properties of the Legendre Transformation

Many of the thermodynamic constraints follow directly from properties of the Legendre transformation (3). We explain some of these properties here, because there has been some confusion in the literature.

The Legendre transform relates tangents in one ensemble to coordinates in the other. For example, a linear segment of $g(x)$ over a finite interval in x will be mapped into a single point y , where $h(y)$ has a kink. Straight segments of $g(x)$ arise from the Maxwell construction and indicate a phase coexistence (mixed phase). For this reason, the grand-canonical phase diagram is much simpler than other ensembles as it consists solely of pure phases.

First we present some relations. Starting with the definitions of the thermodynamic potential densities $\mathcal{E}(n_a, n_b)$ and $-\mathcal{P}(\mu_a, \mu_b)$ defined in (2), we differentiate to find the densities

$$n_a = \frac{\partial \mathcal{P}}{\partial \mu_a} = \beta [\mu_a h(y)]^{3/2} [h(y) - y h'(y)], \quad (\text{A1a})$$

$$n_b = \frac{\partial \mathcal{P}}{\partial \mu_b} = \beta [\mu_a h(y)]^{3/2} h'(y), \quad (\text{A1b})$$

and the chemical potentials

$$\mu_a = \frac{\partial \mathcal{E}}{\partial n_a} = \alpha [n_a g(x)]^{2/3} [g(x) - x g'(x)], \quad (\text{A2a})$$

$$\mu_b = \frac{\partial \mathcal{E}}{\partial n_b} = \alpha [n_a g(x)]^{2/3} g'(x). \quad (\text{A2b})$$

From these relations and the definitions of the asymmetry parameters $x = n_b/n_a$ and $y = \mu_b/\mu_a$, we obtain the

following dictionary. These relations may be used to express $g(x)$ and x in terms of $h(y)$ and y or vice versa:

$$y = \frac{g'(x)}{g(x) - x g'(x)}, \quad h(y) = \frac{1}{g(x) - x g'(x)}, \quad (\text{A3a})$$

$$x = \frac{h'(y)}{h(y) - y h'(y)}, \quad g(x) = \frac{1}{h(y) - y h'(y)}. \quad (\text{A3b})$$

The important geometric property of the Legendre transformation is that it maps tangents in one space to points in the other. Consider the grand-canonical ensemble described by the function $\mathcal{P}(\mu_a, \mu_b)$.¹ The tangents $(\partial_{\mu_a} \mathcal{P}, \partial_{\mu_b} \mathcal{P}) = (n_a, n_b)$ to this function at a point (μ_a, μ_b) in the grand-canonical ensemble map directly to the coordinate (n_a, n_b) in the microcanonical ensemble. Note that the Legendre transformation is symmetric: tangents in the microcanonical ensemble map back to points in the grand-canonical ensemble.

2. Thermodynamic Stability: The Second Law

The thermodynamic potentials follow from a strict minimization procedure over all possible states. If this is properly carried out, the potentials will be convex functions of their arguments. This convexity is the geometric manifestation of the second law. Locally, the requirement is that the Hessian of the potentials—the matrix of second partial derivatives—be positive semi-definite. One can easily show that this requirement also implies that both density and concentration sound modes are stable with corresponding real sound velocities. We shall evaluate now the Hessian's for the thermodynamic potential densities in the case of a two species at unitarity and $T = 0$. We thus find that

$$H(\mathcal{P}_h) \propto \begin{bmatrix} 3(h - y h')^2 + 2y 2h h'' & 3(h h' - y h'^2) - 2y h h'' \\ 3(h h' - y h'^2) - 2y h h'' & 3h'^2 + 2h h'' \end{bmatrix},$$

$$H(\mathcal{E}_g) \propto \begin{bmatrix} 4(g - x g')^2 + 6x 2g g'' & 4(g g' - x g'^2) - 6x g g'' \\ 4(g g' - x g'^2) - 6x g g'' & 4g'^2 + 6g g'' \end{bmatrix},$$

$$H(\mathcal{E}_f) \propto \begin{bmatrix} 10f - 12x f' + 9x^2 f'' & 6f' - 9x f'' \\ 6f' - 9x f'' & 9f'' \end{bmatrix}.$$

The corresponding determinants are:

$$\det[H(\mathcal{P}_h)] \propto h^3 h'' \quad (\text{A4})$$

$$\det[H(\mathcal{E}_g)] \propto g^3 g'' \quad (\text{A5})$$

$$\det[H(\mathcal{E}_f)] \propto 5f f'' - 2f'^2. \quad (\text{A6})$$

From these it is easy to see that the Hessians of \mathcal{P} and \mathcal{E} are positive definite if $h'' \geq 0$ and $h \geq 0$, or $g'' \geq 0$ and $g \geq 0$. If one were to use the parametrization of the

¹ Strictly speaking the grand-canonical potential is $-V\mathcal{P}(\mu_a, \mu_b)$, notice the minus sign, where V is the volume.

energy density \mathcal{E} through f as suggested by Cohen [8] the situation is more complicated, as one would have to satisfy the nonlinear differential constraint

$$5ff'' - 2f'^2 \geq 0, \quad (\text{A7})$$

cf. Eq. (6) in Ref. [8].

Though not related by a strict Legendre transformation, equations (A3) show that the universal functions $g(x)$ and $h(y)$ are similarly related, hence Fig. 2 exhibits the same Maxwell construction properties. Note that the linear Maxwell construction only works with the functional form of $g(x)$ as introduced in (2a): if one uses the function $f(x) = g^{5/3}(x)$ introduced in [8], then the equivalent construction will involve nontrivial forms of $f(x)$ that saturate the inequality (A7) [8]:

$$f(x) = (A + Bx)^{5/3}. \quad (\text{A8})$$

For this reason, the function $g(x)$ is substantially simpler to discuss than $f(x)$. By further requiring saturation of inequality (A7) throughout the entire interval, Cohen [8] obtained

$$f(x) = \{1 + [(2\xi)^{3/5} - 1]x\}^{5/3}, \quad (\text{A9})$$

which describes the case of a vanishing partially polarized region PP_a .

Finally, we discuss the physical significance of kinks in $\mathcal{E}(n)$ which translate to flat regions of $\mathcal{P}(\mu)$ in the grand-canonical ensemble. A kink in $\mathcal{E}(n)$ means that, for a range of tangents (chemical potentials), the energy of the ground state does not change. In other words, the system is insensitive to a range of chemical potentials. For example, the superfluid phase SF is insensitive to a range of chemical potential splitting μ_- because of the physical gap in the spectrum. The flat regions in the grand canonical ensemble represents the same physical state (same densities) that are stable over a range of chemical potentials due to this gap.

As discussed in the main text, the system may or may not respond to chemical potential differences strictly less than the gap $\mu_- < \Delta$, but will definitely respond when $\mu_- > \Delta$. This gave us the bound Y_1 on the transition parameter y_1 (see (A18) below).

3. Maxwell Construction

As an example, let us consider the Maxwell construction for phase coexistence in the microcanonical ensemble with a single species “ a ”. The Maxwell construction for the case of two species at unitarity is somewhat more complicated, but, as we discussed above, involves the same type of linear construction if the function $g(x)$ is used. This ensemble is constructed by minimizing the energy density $\mathcal{E}(n)$ over all phases ρ with fixed total particle number $N = nV$, and volume V :

$$\mathcal{E}(n) = \min_{\rho} \mathcal{E}_{\rho}(N/V). \quad (\text{A10})$$

In the microcanonical ensemble, this procedure is slightly complicated by the possibility of phase coexistence. Consider two distinct pure phases $\rho \in \{1, 2\}$ with given energy densities $\mathcal{E}_1(n)$ and $\mathcal{E}_2(n)$: an example of two such phases is shown in Fig. 4. Minimizing (A10) over these phases separately produces an energy density $\mathcal{E}(n)$ that is not convex. The Maxwell construction proceeds by constructing a series of systems with fixed N by combining a physical fraction z of the system in phase ρ_1 with density n_1 and the remaining fraction $1 - z$ in phase ρ_2 with density n_2 subject to the constraint of fixed average density

$$n = \frac{N}{V} = zn_1 + (1 - z)n_2. \quad (\text{A11})$$

This leaves two degrees of freedom and defines a series of two-component mixed phases that must also be considered in (A10) with energy density:

$$\mathcal{E}(n) = z\mathcal{E}_{\rho_1}(n_1) + (1 - z)\mathcal{E}_{\rho_2}(n_2). \quad (\text{A12})$$

Minimizing $\mathcal{E}(n) - \mu n$, where μ is a Lagrange multiplier, leads to the linear segment shown in bold in Fig. 4, which is the convex hull of the energy densities. More specifically, by varying $n_{1,2}$ and z , (and assuming that all derivatives exists), one obtains the slope

$$\mu_c = \frac{\mathcal{E}_{\rho_1}(n_1) - \mathcal{E}_{\rho_2}(n_2)}{n_1 - n_2} = \frac{\partial \mathcal{E}_{\rho_1}(n_1)}{\partial n_1} = \frac{\partial \mathcal{E}_{\rho_2}(n_2)}{\partial n_2}. \quad (\text{A13})$$

This is simultaneously the slope of the line segment defining the mixed phase, and the tangents to the two energy densities. In the case of the \mathcal{E}_{ρ_2} shown in Fig. 4, the function has a cusp at the point of transition. In this case, $\partial \mathcal{E}_{\rho_2}(n_2)/\partial n_2$ should be interpreted as the appropriate value in the interval defined by the corresponding derivatives computed to the left and to the right of the kink. In (A13) $\partial \mathcal{E}_{\rho_2}/\partial n_2$ may assume any of these values to satisfy the equilibrium condition. This construction

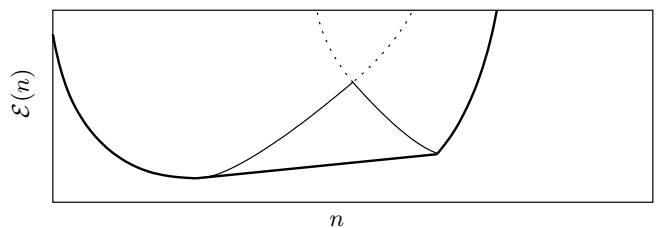


FIG. 4: Maxwell construction for two competing phases in the microcanonical ensemble $\rho \in \{1, 2\}$ with given energy densities $\mathcal{E}_1(n)$ and $\mathcal{E}_2(n)$. The right phase has a gap as signified by the kink. The left phase has no gap. A first-order phase transition connects the two phases. Minimizing (A10) produces the thin solid curve, but this is not convex. The Maxwell construction amounts to finding the convex hull—the thick solid line—which restores the convexity of $\mathcal{E}(n)$ required by the second law of thermodynamics.

guarantees that the potential $\mathcal{E}(n)$ will be convex as required by the second law of thermodynamics.

The conditions of minimization are equivalent to the conditions that the chemical potential and pressure of the two coexisting phases be equal. Note that phase coexistence occurs only along the linear segment. Along this entire segment, the tangent is the same. Thus, the entire region of phase coexistence is described by a single point μ_c representing the phase transition in the grand-canonical ensemble. Furthermore, since the density changes discontinuously from one side of the phase transition to the other, the pressure—though continuous—will have a kink at μ_c , consistent with a first-order transition.

For this reason, phase structures are much simpler when considered in the grand-canonical ensemble. In this ensemble, the phase diagram consists of only pure phases: all phase coexistence (mixtures) occur along first-order phase transitions.

4. Constraints

Here we present a few more details about the extraction of the various constraints in the main text. We start with the bound Y_0 . Recall that the transition is defined by chemical potential μ_b required to keep out species “ b ”. This is bounded by the energy gained by adding the single particle e_0 which we estimate: $\mu_b \leq e_0$. We must relate this to the chemical potential μ_a through the density of the free Fermi sea $n_a = \beta\mu_a^{3/2} \Rightarrow \mu_a = (n_a/\beta)^{2/3} = \alpha n_a^{2/3}$. We now express the constraint $\mu_b \leq e_0$ in terms of y_0 :

$$y_0 = \frac{\mu_b}{\mu_a} \leq \frac{e_0}{\alpha n_a^{2/3}} = Y_0. \quad (\text{A14})$$

The bound Y_1 follows from the constraint $\mu_- \leq \Delta$. To express this in terms of the data, we need to express the chemical potentials in terms of the normalization Fermi energy $\varepsilon_F = \mu_+^{\text{FG}}$ of a free gas of the same density $n_+ = n_a + n_b = 2(2m\mu_+^{\text{FG}})^{3/2}/(6\pi^2)$:

$$\varepsilon_F = \frac{1}{2m} [(3\pi^2)n_+]^{2/3} \quad (\text{A15})$$

The relationship between the density of the symmetric phase SF and the chemical potential μ_+ is determined by the parameter ξ from (5):

$$n_+ = \frac{\partial \mathcal{P}_{\text{SF}}(\mu_+)}{\partial \mu_+} = \frac{2\beta}{\xi^{3/2}} \mu_+^{3/2}. \quad (\text{A16})$$

Thus, we have simply $\varepsilon_F = \mu_+/\xi$. We now express the constraint:

$$\frac{\mu_-}{\varepsilon_F} = \xi \frac{\mu_-}{\mu_+} = \xi \frac{1 - y_1}{1 + y_1} \leq \frac{\Delta}{\varepsilon_F}. \quad (\text{A17})$$

Solving for y_1 gives the constraint

$$y_1 \geq Y_1 = \frac{\xi - \Delta/\varepsilon_F}{\xi + \Delta/\varepsilon_F}. \quad (\text{A18})$$

These constraints transform directly into constraints on the derivatives of $g(x)$ through the dictionary (A3). For example, when $x = 0$ we have

$$y_0 \leq Y_0 \quad \Rightarrow \quad \frac{g'(0)}{g(0)} = g'(0) \leq Y_0, \quad (\text{A19})$$

where we have used the fact that $g(0) = 1$. Likewise at $x = 1$ we have

$$y_1 \geq Y_1 \quad \Rightarrow \quad \frac{g'(1)}{g(1) + g'(1)} \geq Y_1, \quad (\text{A20})$$

which gives a lower bound on $g'(1)$. The upper bound on $g'(1)$ is simply the condition that $y_1 \leq 1$ which we may impose by symmetry:

$$y_1 \leq 1 \quad \Rightarrow \quad \frac{g'(1)}{g(1) + g'(1)} \leq 1. \quad (\text{A21})$$

5. Density Profiles

We consider the following functional form for $g(x)$:

$$g(x) = \begin{cases} g_0 + g'_0 x + ax^2 & \text{where } x \in [0, x_T], \\ c + dx & \text{where } x \in [x_T, 1] \end{cases} \quad (\text{A22})$$

The form of the function has been arbitrarily chosen between 0 and x_T (for simplicity, we chose a quadratic polynomial) with the correct intercept $g(0) = 1$ and slope $g'(0) = y_0$. From this curve, we proceed with the Maxwell construction by finding the line that passes through $(x, g(x)) = (1, g(1))$ and that is tangent to the given curve $g(x_T)$ at the point x_T . The resulting $g(x)$ is shown with solid thick line in Fig. 2 and Fig. 7.

Once this curve is established, one can extract $h(y)$ using Eqs. (A3). The only complication arises when there are kinks or linear segments. In this case, there is a linear segment of $g(x)$ for $x \in [x_T, 1]$. From (A3) we see that, throughout this region, y and $h(y)$ take on only a single value: this is the first-order phase transition y_1 . This will result in a kink in the function $h(y)$ at this location.

To compute the density profiles in a trap, we first parametrize the trap so as to establish the spatial variations of the chemical potential. Let us consider a spherical harmonic trap $V(R) \propto R^2$ and consider the coordinate $\tilde{R} = R/R_{\text{vac}}$ where R_{vac} is the radius of the cloud. The effective chemical potentials are established by (13) once the Lagrange multipliers $\lambda_{a,b}$ are chosen. Once this is done, the functional form of $h(y)$ can be used to directly map the position \tilde{R} to the densities using Eq. (A1). In Fig. 5 we show several trap density profiles with the sample function (A22).

6. Extracting $g(x)$ from Experiment

In principle, once the radial density profiles have been measured to sufficient accuracy, one can extract the func-

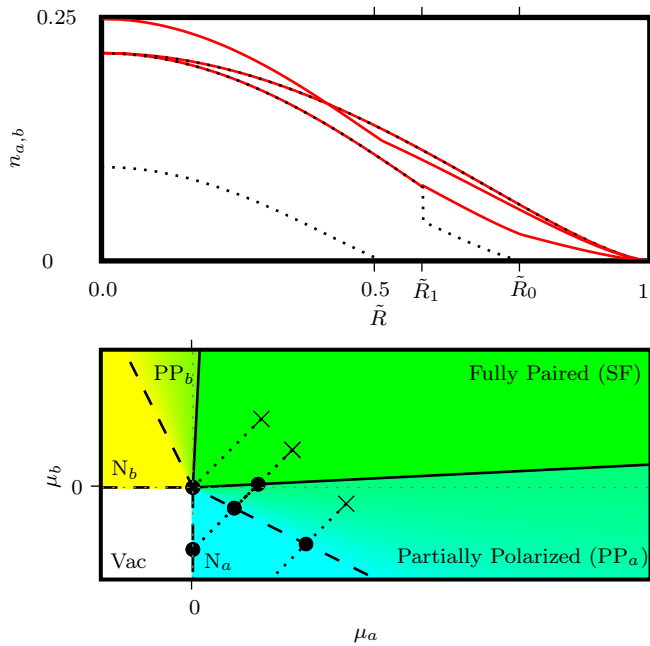


FIG. 5: Density profiles $n_{a,b}$ of the two species in a spherical harmonic trap as a function radius $\tilde{R} = R/R_{\text{vac}}$ in units of the cloud radius R_{vac} for thermodynamic function (A22). Density profiles are plotted for a fixed $\lambda_+ = (\lambda_a + \lambda_b)/2$ and a variety of chemical potential differences $\mu_- = \lambda_-$ ranging from $\lambda_- = 0$ (fully paired $n_a = n_b$ throughout the trap) to $\lambda_- = \lambda_+$ (no superfluid core). The red solid lines are the majority species n_a while the black dotted lines are the minority species. The critical radii for the intermediate profile have been denoted $\tilde{R}_{0,1}$.

tional forms for $g(x)$ and $h(y)$. For example, an experiment can extract the density profiles $n_{a,b}(\mathbf{R})$ (see for example [19]) for a known trapping potential $V(\mathbf{R})$. Using relations (13) and (A2b), we have:

$$g^{2/3}[x(\mathbf{R})]g'[x(\mathbf{R})] = \frac{\mu_b(\mathbf{R})}{\alpha n_a(\mathbf{R})^{2/3}} = \frac{\lambda_b - V(\mathbf{R})}{\alpha n_a^{2/3}(\mathbf{R})}. \quad (\text{A23})$$

This first-order differential equation may be integrated with the boundary condition $g(0) = 1$ to find the function $g(x)$. Finally, λ_b will have to be fit to the trap profile. Note, there are many other ways to extract the same information: we have simply chosen a simple method. Other methods may be less sensitive to experimental errors for example. We leave it to future work to perform this extraction and the accompanying error analysis.

7. Mean Field (Eagles-Leggett) Results

In this section we consider the Eagles-Leggett mean-field model [17]. In this model, one can easily calculate

ξ and Δ (see for example [7]):

$$\xi_{MF} = 0.5906, \quad \frac{\Delta_{MF}}{\varepsilon_F} = 0.6864. \quad (\text{A24})$$

These determine the properties of the superfluid phase SF. If we consider only homogeneous and isotropic phases, then there are three distinct phases: SF, $N_{a,b}$, and N_a .² The SF phase is the usual symmetric BCS-BEC crossover phase, the PP_a phase is a partially polarized two-component Fermi liquid, and the N_a phase is a fully polarized single-component Fermi liquid. One of the shortcomings of the mean-field crossover models is that they neglect the Hartree-Fock contributions.

These terms enter the energy density as $\mathcal{E}_{HF} \approx gn_a n_b$ where g is the coupling constant. In the limit of a short-range interaction, one takes the range of the interaction $r_0 \rightarrow 0$ to zero while holding the vacuum inverse s -wave scattering length a^{-1} fixed.³ This requires that the interaction strength be taken to zero $g \sim \pi r_0/m \rightarrow 0$. The densities $n_{a,b}$ contain no singularities and so the Hartree-Fock contributions vanish. These contributions may be included in weak coupling by resumming particle-particle ladders to obtain $\mathcal{E}_{HF} \approx 4\pi\hbar^2 a n_a n_b/m$, but this procedure may not be extrapolated to unitarity.

Thus, in mean-field, the partially polarized state simply has the pressure of two independent free Fermi gases:

$$\mathcal{P}_{FG_2}(\mu_a, \mu_b) = \frac{2}{5}\beta \left(\mu_a^{5/2} + \mu_b^{5/2} \right). \quad (\text{A25})$$

Pressure equilibrium thus determines the phase transitions in this model and we have the two conditions

$$\mathcal{P}_{FG_2}(\mu_a, y_0^{MF} \mu_b) = \mathcal{P}_{FG}(\mu_a), \quad (\text{A26a})$$

$$\mathcal{P}_{FG_2}(\mu_a, y_1^{MF} \mu_b) = \mathcal{P}_{SF}(\mu_+). \quad (\text{A26b})$$

These imply trivially that $y_0^{MF} = 0$. Since the Hartree-Fock terms vanish, there is no interaction energy and the phase transition between N_a and PP_a occurs for $\mu_b = 0$. The SF/ PP_a transition at y_1 is governed by condition (A26b). Using Eq. (5) and $\mu_b = y_0 \mu_a$, we have

$$2\xi_{MF}^{-3/2} \left(\frac{1 + y_1^{MF}}{2} \right)^{5/2} = 1 + (y_1^{MF})^{5/2}. \quad (\text{A27})$$

This may be solved numerically using Eq. (A24) to obtain $y_1^{MF} = 0.1067$. To summarize: In the Eagles-Leggett mean-field crossover model with homogeneous and isotropic phases, we have:

$$y_0^{MF} = Y_0^{MF} = 0, \quad y_c^{MF} = 0.1051, \quad (\text{A28a})$$

$$Y_1^{MF} = -0.0750, \quad y_1^{MF} = 0.1067. \quad (\text{A28b})$$

² There is the possibility that other phases, like LOFF, compete with the partially polarized phase $N_{a,b}$. In the mean-field model it is unlikely that these phases will drastically alter the locations of the phase transitions. The LOFF-like regions are always very thin, and we neglect these possibilities here.

³ The $a^{-1} = 0$ limit at unitarity does not represent a singularity.

Obviously the lower bound Y_1^{MF} is useless for our purposes.

8. Calculation of e_0

The Hamiltonian describing a system of N_a species “a” fermions interacting with one additional species “b” fermion is:

$$\hat{\mathbf{H}} = \hat{\mathbf{H}}_a + \hat{\mathbf{H}}_0 = \left(\sum_{n=1}^{N_a} \hat{\mathbf{T}}_n \right) + \left(\hat{\mathbf{T}}_0 + \sum_{n=1}^{N_a} \hat{\mathbf{V}}_{n,0} \right), \quad (\text{A29})$$

where $\hat{\mathbf{T}}_k$ are the corresponding kinetic energy operators and $\hat{\mathbf{V}}_{n,0}$ is the potential between the fermion of species “a” with coordinate \mathbf{r}_n with the fermion of species “b” with coordinate \mathbf{r}_0 . Recall that we use the variational wave function (10)

$$\Psi(\mathbf{r}_0; \{\mathbf{r}_n\}) = \Phi_{\text{SD}}(\{\mathbf{r}_n\})\phi(\mathbf{r}_0; \{\mathbf{r}_n\}), \quad (\text{A30})$$

where (8)

$$\phi(\mathbf{r}_0; \{\mathbf{r}_n\}) = \sum_n A_n \frac{\exp(-\kappa r_{0n})}{r_{0n}} \quad (\text{A31})$$

is an eigenfunction of the operator $\hat{\mathbf{H}}_0$:

$$\hat{\mathbf{H}}_0\phi(\mathbf{r}_0; \{\mathbf{r}_n\}) = -\frac{\hbar^2\kappa^2(\{\mathbf{r}_n\})}{2m}\phi(\mathbf{r}_0; \{\mathbf{r}_n\}). \quad (\text{A32})$$

The Slater determinant is of course an eigenfunction of $\hat{\mathbf{H}}_a$:

$$\hat{\mathbf{H}}_a\Phi_{\text{SD}}(\{\mathbf{r}_n\}) = E_{FG}\Phi_{\text{SD}}(\{\mathbf{r}_n\}). \quad (\text{A33})$$

Two additional terms arise from $\hat{\mathbf{H}}_a$ acting on the product wave function. The first term is a cross-derivative

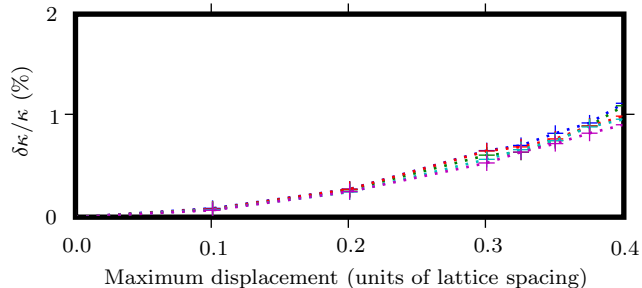


FIG. 6: Relative change in κ for randomly perturbed bcc lattices. The abscissa shows the maximum deviations each lattice site was displaced from equilibrium as a fraction of the lattice spacing. Curves are shown for cubic lattices from 10 to 14 sites per side. Each curve shows the maximum deviation over a sample of 30 random lattice configurations.

which arises from applying $\hat{\mathbf{H}}_a$ to both the Slater determinant and $\phi(\mathbf{r}_0; \{\mathbf{r}_n\})$. This gives a vanishing contribution, since the integral over momenta

$$\frac{\hbar^2}{m} \int_{k < k_F} \frac{d\mathbf{k}}{(2\pi)^3} \int \prod_{j=0}^{N_a} d\mathbf{r}_j \sum_{l=1}^{N_a} (i\mathbf{k} \cdot \nabla_l) \phi^2(\mathbf{r}_0; \{\mathbf{r}_n\}) \quad (\text{A34})$$

is identically zero because of the symmetry of the Fermi sea. The second kind of term is due to $\hat{\mathbf{H}}_a$ acting on $\phi(\mathbf{r}_0; \{\mathbf{r}_n\})$ and which pulls down derivatives of $\kappa(\{\mathbf{r}_n\})$ and $A_n(\{\mathbf{r}_n\})$:

$$\hat{\mathbf{H}}_a\phi(\mathbf{r}_0; \{\mathbf{r}_n\}) = -\frac{\hbar^2\kappa^2(\{\mathbf{r}_n\})}{2m}\phi(\mathbf{r}_0; \{\mathbf{r}_n\}) + \text{derivative corrections.} \quad (\text{A35})$$

In what follows, we neglect the derivative corrections, but, as we discuss below, we expect these to be small. Within this approximation, the expectation value of this Hamiltonian is

$$\langle \Psi | \hat{\mathbf{H}} | \Psi \rangle = E_{FG} + e_0 = E_{FG} - \frac{\hbar^2\kappa^2}{m} \quad (\text{A36})$$

where E_{FG} is the ground state energy of the system of N_a fermions alone. This contribution arises by applying $\sum_{n=1}^{N_a} T_n$ to the Slater determinant alone. It is implied here that $\phi(\mathbf{r}_0; \{\mathbf{r}_n\})$ is normalized.

We have checked explicitly that at unitarity for several simple lattice configurations (fcc, bcc) and for configurations in which the positions of all the fermion species “a” were randomly changed from the ideal lattice configurations within the Fermi hole, the values of κ varied by a few percent at most, see Fig. (6). This analysis thus confirms our assumption that the fluctuations in a free Fermi gas of the number density $n_a(\mathbf{r})$ do not affect in a noticeable manner the value of κ .

For comparison, we replot the function $g(x)$ from Fig. 2 and include the Monte Carlo data from [20]. The authors of Ref. [20] simulated a two-component polarized normal Fermi gas, which provides a variational bound on the energy. We thank S. Giorgini for sending us their numerical results [20].

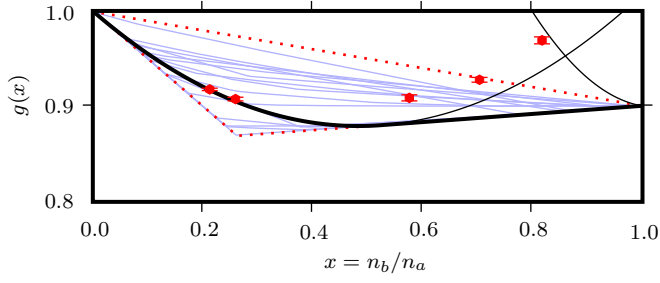


FIG. 7: Monte Carlo variational upper bound on $g(x)$ from [20] plotted on top of the function $g(x)$ from our Figure 2. Note the agreement from small polarizations indicating that our estimate for Y_0 is consistent with their proper variational bound. For larger polarizations, the true curve will lie below the results of Ref. [20] for two reasons: 1) The Maxwell construction for $g(x)$ (see Fig. (2) of [20]) and 2) The authors of Ref. [20] considered only normal Fermi partially polarized states. As shown in [12], at $T = 0$, partially polarized states will be superfluid. This could noticeably lower the energy for substantial polarizations at unitarity.